ADVANCED OPTICAL MATERIALS
www.advopticalmat.de

Deformed Honeycomb Lattices of InGaAs Nanowires Grown on Silicon-on-Insulator for Photonic Crystal Surface-Emitting Lasers

Cristian Messina, Yongkang Gong, Oumaima Abouzaid, Bogdan-Petrin Ratiu, Tim Grieb, Zhao Yan, Andreas Rosenauer, Sang Soon Oh, and Qiang Li**

Photonic crystals can be used to achieve high-performance surface-emitting lasers and enable novel photonic topological insulator devices. In this work, a GaAs/InGaAs heterojunction nanowire platform by selective area metalorganic vapor phase epitaxy for such applications is demonstrated. The nanowires are arranged into deformed honeycomb lattices on silicon-on-insulator substrate to exploit the quadrupolar photonic band-edge mode. Core–shell and axial heterostructures are formed with their crystalline properties studied by scanning transmission electron microscopy. Room-temperature, single mode lasing from both stretched and compressed honeycomb lattices within the telecom-O band, with lasing threshold as low as 1.25 μJ cm^{-2} is demonstrated. The potential of using InGaAs nanowire-based honeycomb lattices for small-divergence surface-emitting lasers and topological edge mode lasers is investigated. Finite-difference time-domain far field simulations suggest a sub-10° beam divergence can be achieved thanks to the out-of-plane diffraction.

1. Introduction

Recent developments in photonic crystal (PhC)-based lasers have demonstrated superior performance to commonly used vertical cavity surface-emitting lasers (VCSELs) and edge emitting lasers.[1–4] The single-mode operation, high modulation frequency and brightness,[5,6] and symmetric beam profiles with excellent narrow beam divergence[7] make them highly promising for light detection and ranging[8] and optical sensing applications. Conventionally, top-down nanofabrication processes are used for fabricating PhC surface-emitting lasers (PCSELs) as well as emerging topological cavity surface-emitting lasers.[9–12] Over the last few years, selective area, catalyst-free growth of nanowires has progressed rapidly, providing a unique platform for ultracompact bottom-up PhC lasers.[13–16] In comparison to top-down etched PhC cavities, the vertical and atomically flat sidewall surface and the ability to form in situ passivation layers in nanowire growth minimize scattering and propagation losses and thereby preserve high radiative recombination efficiency. By breaking or relaxing the constraints from materials lattice mismatch, combining dissimilar materials into 3D axial and core–shell structures with strong quantum confinement and direct epitaxial integration on technologically important substrates such as silicon-on-insulator (SOI) chips also become possible. Optically pumped lasing from a lift-off 2D GaAs/InGaAs/GaAs nanowire arrays was realized emitting at wavelengths between 960 and 989 nm.[17] Near vertical surface emission around 850 nm from an InP nanowire PhC structure on InP substrate was recently reported, exhibiting pulse lasing at room temperature as well as continuous-wave lasing at 77 K with an output power of 470 μW.[18] Electrically pumped surface-emitting laser diodes using bottom-up PhC cavities have so far only been achieved by InGaN/AlGaN nanowires[1] and remain one of the biggest challenges in III-As/P based nanowires. For practical integration of nanowire lasers with silicon photonic integrated circuits and silicon electronics, direct growth of nanowire lasers on silicon operating in the relevant telecom spectral bandwidth (1.3–1.55 μm) is crucial. To date, this has been developed using either bandgap tunable InGaAs nanowire-based 1D or 2D PhC arrays[15,19–21] or strain-compensated InGaAs/(In,Al)GaAs multiquantum-well nanowires.[22] Despite impressive waveguide-coupled lasing at room temperature and low-threshold characteristics that have been demonstrated, a surface-emitting telecom wavelength nanowire PhC laser, which could be of great interest for optical sensing applications, has not been reported yet.

C. Messina, Y. Gong, O. Abouzaid, B.-P. Ratiu, Z. Yan, S. S. Oh, Q. Li
School of Physics and Astronomy
Cardiff University
Cardiff CF24 3AA, UK
E-mail: OhS2@cardiff.ac.uk; LiQ44@cardiff.ac.uk
T. Grieb, A. Rosenauer
Institute of Solid State Physics
University of Bremen
28359 Bremen, Germany

The ORCID identification number(s) for the author(s) of this article can be found under https://doi.org/10.1002/adom.202201809.

DOI: 10.1002/adom.202201809

In this work, we demonstrate GaAs/InGaAs nanowires selectively grown on SOI substrate as a material platform for surface-emitting telecom lasers and potential topological cavity lasers. In contrast to a square lattice which uses off-Γ symmetry points,[15,23] these nanowires are arranged into deformed honeycomb lattices to access Γ point band edge modes for highly directional vertical emission. Our fully integrated, bottom-up approach allows to completely define the geometry of the system through control of the growth parameters and to achieve atomically smooth side facets, minimizing light scattering in the cavity. We experimentally demonstrate that lasing occurs at the Γ point band-edge of the honeycomb photonic band structures, with lasing wavelengths reaching the telecom O-band. With the aid of numerical simulations, we discuss the potential of employing these highly uniform, lithographically defined nanowire arrays for achieving small angle divergence PCSELs and designing novel topological cavity lasers.

2. Modeling and Growth

First, we consider a 2D PhC structure based on an ideal honeycomb lattice composed of core–shell GaAs/InGaAs/InGaP nanowires on an SOI substrate, as shown in **Figure 1**a,b. The honeycomb lattice can be obtained by placing hexagonal unit cells with side length R at the lattice sites of a hexagonal lattice defined by the basis vectors $\vec{a}_1$ and $\vec{a}_2$ and the lattice constant a given as $|\vec{a}_1| = |\vec{a}_2|$ (see Figure 1c). This PhC lattice natively presents a photonic band structure with a double Dirac cone, which is folded back from K and K' points, at the Γ point in momentum space for transverse-magnetic (TM) modes.[24] This degeneracy can be lifted by stretching or compressing the edge length $R = a/3$, thereby preserving the hexagonal unit cell shapes so that the photonic bands exhibit characteristic electron p and d orbital-like electric field profiles. Here, we consider the stretched honeycomb lattice, with unit cells comprised of 12 InGaAs nanowires (n = 3.6) cladded between an SOI substrate and air. Photonic band structures and mode profiles were calculated using the guided mode expansion method[25] and confirmed via finite-difference time-domain (FDTD) simulations. We model the lattice parameters such that the bottom band-edge mode has a frequency at the Γ point matching the telecom O-band wavelength. With parameters of a = 640 nm and R = 230 nm, the bottom band-edge has a frequency of $\omega = 0.50 \times 2\pi c/a$ (λ = 1280 nm) as shown in Figure 1d. It is also noted this band-edge mode presents a quadrupole mode, as indicated by the in-plane and cross-sectional electric field profiles in Figure 1e, resulting from the dipole and quadrupole band-inversion in the stretched honeycomb lattice.[9,24] The overlap of the quadrupole mode with the gain material is as

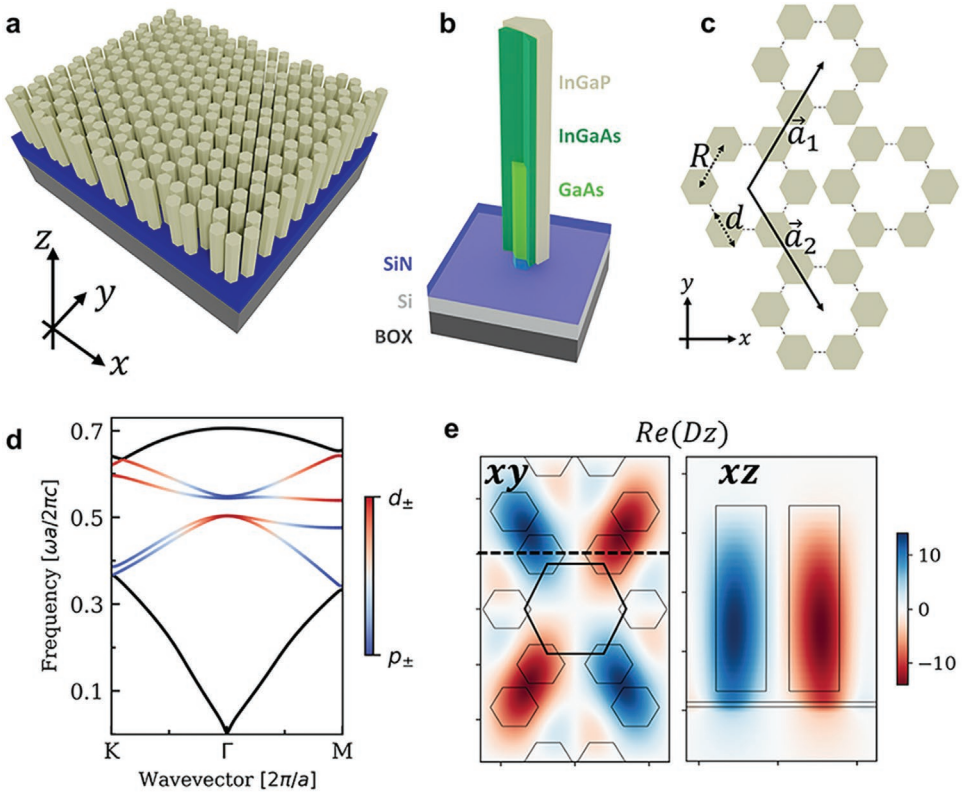

Figure 1. Design of the nanowire-based PCSEL. a) Schematic of the honeycomb nanowire array on the SOI substrate. b) The core–shell structure of the nanowire on SOI substrate with a thin SiN mask. The nanowire consists of a GaAs core that extends into the SOI through the SiN mask, an InGaAs active layer, and a thin InGaP shell. c) Top-down view of the nanowire honeycomb lattice with lattice constant a. The nanowires of diameter d are arranged into hexagonal unit cells of edge length R. d) Photonic band structure of the stretched honeycomb lattice for transverse-magnetic (TM) modes, calculated using a guided mode expansion method: blue and red, respectively, indicate the dipole and quadrupole bands. e) Quadrupole-like electric field profiles in the z-normal (left) and y-normal (right) planes, calculated at the bottom band-edge.

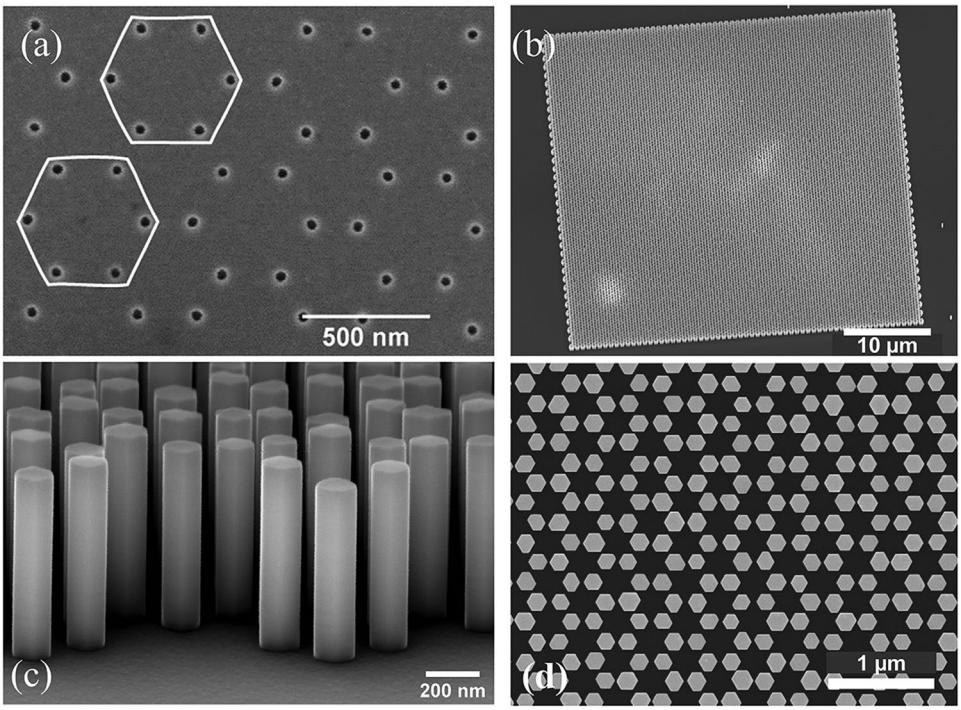

Figure 2. a) Top-view SEM image of the initial nanohole array. b) Tilted view SEM image of a 40 × 40 µm^2 nanowire array. c) Zoom-in tilted view SEM image of the nanowires. d) Top view SEM image showing the hexagonal cross-sections of the nanowires.

high as 40%. Since the mode group velocity $d\omega/dk$ vanishes at the band edge, the increased interaction time with the active gain material leads to gain enhancement.[1,26]

The nanowires were grown using selective-area metalorganic vapor phase epitaxy (MOVPE). We started from a (111) SOI wafer with a thick buried oxide and a Si top layer which was thinned down to a nominal thickness of 40 nm for better optical confinement in the vertical direction. A 20 nm SiN layer was deposited using plasma-enhanced chemical vapor deposition as the growth mask. The substrate was patterned using electron-beam lithography and etched to expose the thin Si layer in circular nanoholes as small as 30 nm in diameter, as shown by a top-view scanning electron microscopy (SEM) image in **Figure 2**a. The nanoholes are arranged into ideal, stretched, and compressed honeycomb lattices. Prior to nanowire growth, the patterned substrate was cleaned using a diluted hydrofluoric acid solution to remove native oxide on the silicon surface and then transferred into the reactor chamber immediately. Annealing in the MOVPE reactor at a wafer surface temperature of 850 °C in hydrogen was carried out to desorb any residual oxide and prepare the silicon surface for III–V nucleation. The precursors used for nanowire growth are triethylgallium, trimethylindium, tertiarybutylarsine, and tertiarybutylphosphine. GaAs core nanowires were grown first from the Si surface at 680 °C under a V/III ratio of 82. The growth temperature was then reduced to 610 °C for growing InGaAs under a V/III ratio of 40 and an In/III vapor supply of 40%. We expect InGaAs will grow faster vertically with some lateral overgrowth surrounding the GaAs core, which is confirmed by transmission electron microscope (TEM) and will be discussed shortly. Finally, The GaAs/InGaAs nanowires were capped by 15 nm InGaP shells to reduce nonradiative surface recombination and improve the radiation efficiency. The reason of growing the GaAs stem is twofold. First, starting with a GaAs seeding layer significantly improves the yield and uniformity of nanowire growth on silicon. Second, the refractive index difference in the GaAs/InGaAs heterostructure improves optical confinement and mitigates optical field leakage into the silicon substrate.

3. Results and Discussion

After selective area epitaxy (SAE), we achieved ≈100% yield over nanowire arrays as large as 60 × 60 µm^2 with good uniformity. A tilted view SEM image of a 40 × 40 µm^2 nanowire array is displayed in Figure 2b, with a zoom-in image in Figure 2c showing atomically flat sidewalls along the $\{1\bar{1}0\}$ planes. Figure 2d shows a top-view SEM image of the nanowires indicating some variations of their hexagonal cross-sections. The measured height H and diameter d of the nanowires from SEM are 630 ±10 and 163 ± 8 nm, respectively. With increased nanohole diameter from 30 to 40 and 50 nm, the likelihood of neighboring nanowires merging into fin-like structures[27] increases by four and six times, respectively. We also noted the effect of different nanowire array sizes on the nanowire dimensions. For 40 × 40, 50 × 50, and 60 × 60 µm^2 arrays, there was a slight decrease in nanowire diameter from 176 to 170 to 163 nm, which we attribute to the group-III limited diffusion dynamics in SAE.

To confirm the material composition, thickness, and crystalline structure, we then performed high-angle annular dark field scanning transmission electron microscopy (HAADF-STEM) and energy dispersive X-ray spectroscopy (EDX). This was done

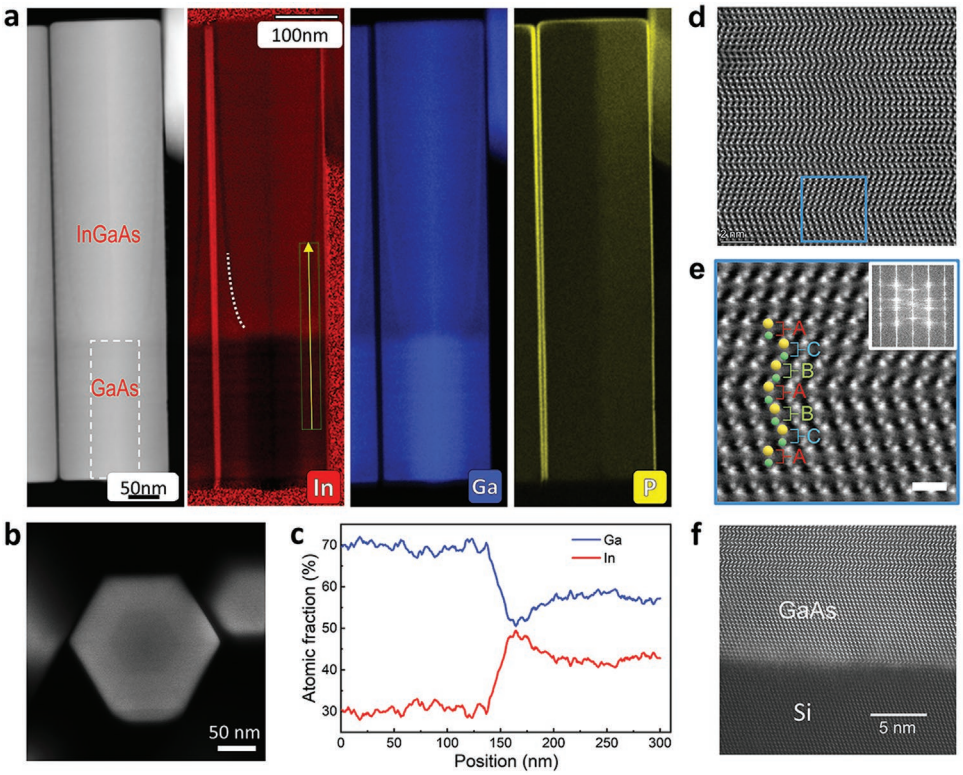

Figure 3. TEM characterization. Panels (a)–(e) are acquired by transferring the nanowires to TEM graphene grid using a micromanipulator. Panel (f) is acquired by preparing a TEM lamella by FIB along ⟨110⟩ zone axis. a) STEM-HAADF image acquired in ⟨112⟩ zone axis and EDX elemental maps (net peak intensities). b) STEM-HAADF image viewed at the nanowire base. c) Line profile of the In and Ga composition from EDX at the InGaAs shell. The scanned region is indicated by the yellow arrow in the In map in (a). d) STEM-HAADF image acquired in ⟨110⟩ zone axis at the InGaAs region of the nanowire. e) Magnified image of the blue box in (d), demonstrating the ABC-type stacking. Scale bar, 1 nm. The yellow sphere represents group III atoms and green represents As atoms. The inset shows an FFT image of the nanowire. f) STEM-HAADF image acquired in ⟨110⟩ zone axis at the Si/GaAs interface.

by breaking nanowires off the SOI substrate from the SiN mask openings and then placing the wires on the TEM graphene grid using a micromanipulator in an SEM. From the EDX mapping of **Figure 3**a, the GaAs core is with ≈80 nm diameter and 230 nm height. The InGaAs layer exhibits pronounced axial growth from the top (111)B facet of GaAs as well as considerable radial growth (≈45 nm) from the six side-faces, forming a coaxial core–shell structure at the bottom. The contrast in the EDX mapping suggests different indium incorporation in axial and radial growth. In catalyst-free SAE nanowires, growing core–shell structures with lattice mismatched materials often lead to shell nonuniformity or nanowire bending as a result of the Stranski–Krastanov (SK) 3D island growth mode induced by the misfit strain.[28–31] Here, we are able to achieve uniform growth of InGaAs shell around the GaAs core while maintaining the hexagonal nanowire morphology, which is further verified by the cross-sectional HAADF-STEM image taken from the nanowire base shown in Figure 3b. We believe the demonstrated strained GaAs/InGaAs heterostructure here can add additional flexibility in engineering nanowire heterojunction devices. From our simulation studies, the GaAs core of 230 nm height is beneficial in elevating the optical mode and mitigating light leakage to the Si device layer. Future work will follow to further increase the indium composition to extend emission wavelength into telecom C-band and embed strained InGaAs multi-quantum-well structures into the nanowires. The EDX line profile in Figure 3c displays a lower indium composition (around 15% lower) at the InGaAs bottom shell as compared to the InGaAs main layer formed above the height of GaAs (the EDX scanning area is indicated by the yellow arrow in the indium mapping of Figure 3a). We speculate this could be attributed to the different strain experienced by the InGaAs layer in radial and axial growth. The contrast in Figure 3b also indicates a lower indium composition along the six ⟨112⟩ direction lines from the GaAs core. This has been widely observed in other reported coaxial nanowires where a self-ordering effect reduces indium incorporation at the nanowire corners.[32] It also explains the dark lines observed in the side-view EDX mapping for indium in Figure 3a (marked in the In map in Figure 3a by a dashed line as a guide to the eye) which originate from the corners of the GaAs hexagon and rise up as the InGaAs growth takes place along both vertical and lateral directions. An atomically resolved image along the ⟨110⟩ zone axis is displayed in Figure 3d. The InGaAs exhibits a zincblende phase with high density twins as confirmed by the revealed "ABC" type stacking and the fast Fourier transform (FFT) image in Figure 3e.[33–35] Another thinned TEM lamella was also prepared using focused ion beam (FIB) to inspect the GaAs/Si interface in the mask opening, as shown

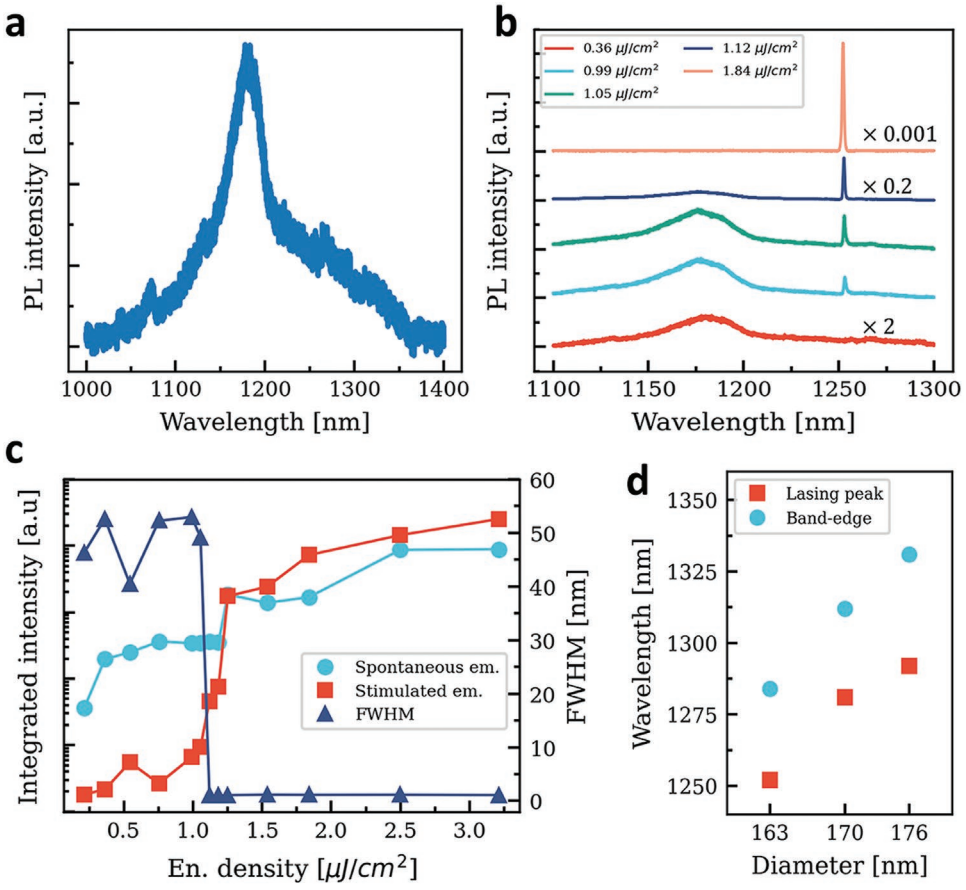

Figure 4. Room-temperature optical characterization of the nanowire arrays. a) Spontaneous photoluminescence emission obtained at a low pump power of 0.21 μJ cm^{-2}. b) Photoluminescence emission at increasing pump powers, showing single-mode lasing at 1252 nm. c) Integrated emission intensities of the stimulated emission (red squares), spontaneous emission (cyan circles), and peak FWHM (blue triangles). d) Lasing frequencies for three nanowire arrays with different nanowire diameters (red squares) and calculated band-edge frequencies for the same arrays (cyan circles).

by the high-resolution STEM image in Figure 3f. A 7 nm thick defect-free region was found above the GaAs/Si hetero-interface, followed by high density twinning through the wire.

To characterize the as-grown nanowire arrays on SOI substrate for PCSELs, we optically pumped a stretched honeycomb nanowire array with pulsed excitation using room-temperature micro-photoluminescence (PL) spectroscopy. A supercontinuum source with a 633 nm laser wavelength and ≈100 ps pulse width at a 5 MHz repetition rate was used, illuminating the cavity from the top with a beam size of ≈6 μm in diameter. The cavity emission was collected from the top and analyzed using an InGaAs focal plane array detector connected to a spectrometer. We measured the PL emission at different pump powers. At a low excitation power, as shown in **Figure 4**a, a broad spontaneous emission appears between 1100 and 1300 nm and peaked at 1179 nm, corresponding to an indium solid phase composition of 0.27.[36] Increasing the pump power, a sharp lasing peak appears at 1252 nm and quickly dominates the spontaneous emission (Figure 4b). Accordingly, the peak full-width at half-maximum (FWHM) quickly drops to 1.1 nm around the threshold of 1.25 μJ cm^{-2} (Figure 4c). A slight blue-shift in the spontaneous emission peak, from 1179 to 1175 nm, is also observed at increased pump power, due to the band-filling effect. The lasing threshold fluence here is among the lowest reported values from bottom up nanowire PhC lasers.[15,17–20] Further improved performance is expected with better overlapping of the gain material wavelength and the cavity resonance wavelength. We observe that the lasing wavelength closely matches the quadrupole bottom band-edge wavelength in our model. To confirm that the band-edge quadrupole mode is being excited, we calculated the band-edge frequency shift as the nanowire diameter increases and compared it against the observed lasing wavelengths from experimental samples. As shown in Figure 4d, with nanowire diameter increasing from 163 to 170 and 176 nm, the lasing wavelength follows the same trend as predicted by the band-edge modeling. This agrees well with the overall increase in volume-averaged refractive index. The ≈30 nm wavelength difference between the simulated band-edge and the lasing wavelength can be attributed to fabrication imperfections.

Since light confined in the PhC plane undergoes coherent oscillation and is coupled to the vertical direction through first-order Bragg diffraction,[37] we expect the lasing emission from the PCSEL device to achieve narrow divergence. In **Figure 5**a, we consider the far field projection resulting from a PhC area of 35 μm^2, equal to the optical pumping beam size experimentally

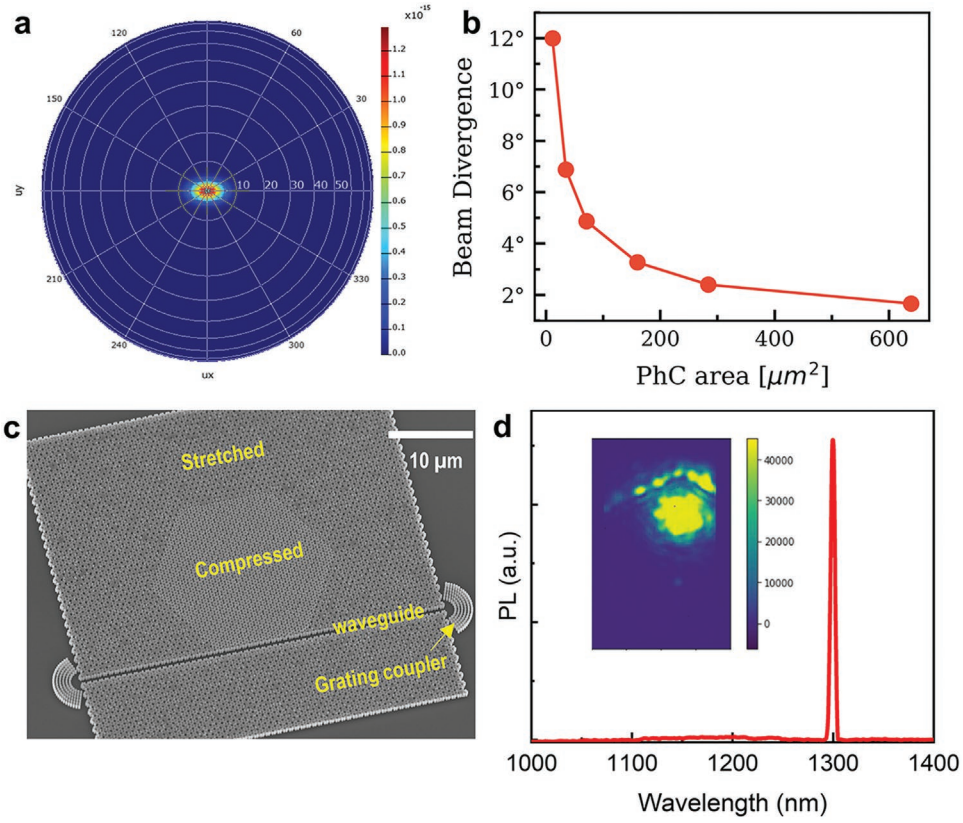

Figure 5. a) Far field projection for a cavity of 35 μm², resulting in sub-10° beam divergence. b) Beam divergence angle as a function of simulated PhC cavity area. c) SEM image of a hexagonal shape topological cavity with a PhC waveguide and grating couplers. d) PL spectrum of band edge mode lasing from the compressed honeycomb PhC when the inside of the hexagonal cavity (compressed) is pumped. (inset) Optical image of the lasing emission.

used to achieve lasing. In our model, coherent oscillation from this area is enough to achieve sub-10° beam divergence. Figure 5b further plots the beam divergence as a function of the PhC cavity area by increasing the number of unit cells in the FDTD modeling. The beam divergence angle drops quickly with increasing PhC cavity area, approaching 3° divergence with PhC area over 60 μm². In practice, however, in-plane coherence is expected to be limited by fabrication imperfections, and beam-widening effects such as thermal lensing also need to be considered.[38] Experimental measurement of the beam divergence, e.g., via back focal plane or Fourier plane imaging and spectroscopy, and fabricating electrically injected PCSELs for practical applications will be pursued in future work.

In addition to PCSEL devices, the ability to grow deformed honeycomb nanowire arrays in a single epitaxy provides a promising platform for building topological cavities. Figure 5c shows the SEM image of a hexagonal-shaped cavity by combining the compressed and stretched honeycomb nanowire lattices into a single device to generate topological interface modes. Although we are able to achieve PhC band edge mode lasing at 1300 nm coming from the compressed honeycomb lattice inside the hexagonal cavity, as shown in Figure 5d, topological edge mode lasing or topological bulk mode lasing[9] is yet to be realized. Further investigations will be needed to selectively excite the topological edge mode in a system where band-edge modes and PhC bulk modes are also present.

4. Conclusion

In conclusion, we have demonstrated a bottom-up InGaAs nanowire platform on SOI substrate for PhC surface-emitting lasers at telecom wavelengths. The nanowires are arranged into deformed honeycomb lattices using lithographically defined SAE to take advantage of the Γ point band-edge modes for high directional vertical emission. Through modeling and optical pumping of the cavity, we have demonstrated room-temperature, very low threshold lasing from both stretched and compressed honeycomb lattices, with far field simulations suggesting an angle divergence smaller than 10°. Our bottom-up approach can also be extended to other PhC cavity devices, including the topological bulk- and edge-mode lasers, that despite achieving remarkably superior performance to commercial VCSELs, have been challenging to fully integrate on Si to date.

5. Experimental Section

Nanowire Characterization: The sample was analyzed by STEM in a Thermo Fisher Spectra 300 TEM at an acceleration voltage of 300 kV. EDX was performed in STEM mode using a Thermo Fisher Super-X detector. The Thermo Fisher Velox software was used to analyze the EDX data.

Optical Characterization: The nanowire arrays were optically pumped at room temperature by a pulsed supercontinuum laser (model YSL

SC-PRO 7) with 633 nm peak wavelength, ≈100 ps pulse width, and 5 MHz repetition rate. Normal incidence was employed in the micro-PL set up, in which the pumping source and the sample emission were focused and collected through a 50× Mitutoyo Plan Apo NIR Infinity Corrected Objective (NA = 0.65, 0.42 µm resolving power) and analyzed using a NIRvana 640 InGaAs focal plane array detector connected to a spectrometer (Acton SpectraPro SP-2750). The emission patterns from the nanowire arrays were captured by the 2D InGaAs detector.

Acknowledgements

This work was supported by the Engineering and Physical Sciences Research Council (grant number EP/T01105X/1), the European Regional Development Fund through the Welsh Government (80762-CU145 (East)), and the Future Compound Semiconductor Manufacturing Hub (grant number EP/P006973/1).

Conflict of Interest

The authors declare no conflict of interest.

Data Availability Statement

The data that support the findings of this study are available from the corresponding author upon reasonable request.

Keywords

III–V semiconductors, nanowires, photonic crystals, selective area epitaxy, surface-emitting lasers

Received: August 2, 2022
Revised: November 16, 2022
Published online:

[1] Y. H. Ra, R. T. Rashid, X. Liu, S. M. Sadaf, K. Mashooq, Z. Mi, *Sci. Adv.* **2020**, *6*, eaav7523.
[2] M. Yoshida, M. de Zoysa, K. Ishizaki, Y. Tanaka, M. Kawasaki, R. Hatsuda, B. Song, J. Gelleta, S. Noda, *Nat. Mater.* **2018**, *18*, 121.
[3] D. M. Williams, K. M. Groom, B. J. Stevens, D. T. D. Childs, R. J. E. Taylor, S. Khamas, R. A. Hogg, N. Ikeda, Y. Sugimoto, *IEEE Photonics Technol. Lett.* **2012**, *24*, 966.
[4] Z. Bian, K. J. Rae, A. F. McKenzie, B. C. King, N. Babazadeh, G. Li, J. R. Orchard, N. D. Gerrard, S. Thoms, D. A. Maclaren, R. J. E. Taylor, D. Childs, R. A. Hogg, *IEEE Photonics Technol. Lett.* **2020**, *32*, 1531.
[5] T. Inoue, M. Yoshida, M. D. Zoysa, K. Ishizaki, S. Noda, S. Noda, *Opt. Express* **2020**, *28*, 5050.
[6] K. Hirose, Y. Liang, Y. Kurosaka, A. Watanabe, T. Sugiyama, S. Noda, *Nat. Photonics* **2014**, *8*, 406.
[7] M. Imada, S. Noda, A. Chutinan, T. Tokuda, M. Murata, G. Sasaki, *Appl. Phys. Lett.* **1999**, *75*, 316.
[8] R. Sakata, K. Ishizaki, M. de Zoysa, S. Fukuhara, T. Inoue, Y. Tanaka, K. Iwata, R. Hatsuda, M. Yoshida, J. Gelleta, S. Noda, *Nat. Commun.* **2020**, *11*, 3487.
[9] Z. K. Shao, H. Z. Chen, S. Wang, X. R. Mao, Z. Q. Yang, S. L. Wang, X. X. Wang, X. Hu, R. M. Ma, *Nat. Nanotechnol.* **2020**, *15*, 67.
[10] Y. Gong, S. Wong, A. J. Bennett, D. L. Huffaker, S. S. Oh, *ACS Photonics* **2020**, *7*, 2089.
[11] C. Schuller, F. Klopf, J. P. Reithmaier, M. Kamp, A. Forchel, *Appl. Phys. Lett.* **2003**, *82*, 2767.
[12] L. Yang, G. Li, X. Gao, L. Lu, *Nat. Photonics* **2022**, *16*, 279.
[13] K. Tomioka, K. Ikejiri, T. Tanaka, J. Motohisa, S. Hara, K. Hiruma, T. Fukui, *J. Mater. Res.* **2011**, *26*, 2127.
[14] J. Noborisaka, J. Motohisa, T. Fukui, *Appl. Phys. Lett.* **2005**, *86*, 213102.
[15] W. Lee, H. Kim, J. You, D. L. Huffaker, *Sci. Rep.* **2017**, *7*, 9543.
[16] Z. Azimi, A. Gopakumar, L. Li, F. Kremer, M. Lockrey, A. A. Wibowo, H. T. Nguyen, H. H. Tan, C. Jagadish, J. Wong-Leung, *Adv. Opt. Mater.* **2022**, *10*, 2200739.
[17] A. C. Scofield, S. Kim, J. N. Shapiro, A. Lin, B. Liang, A. Scherer, D. L. Huffaker, *Nano Lett.* **2011**, *11*, 5387.
[18] C. Tu, M. Fränzl, Q. Gao, H. Tan, C. Jagadish, H. Schmitzer, H. P. Wagner, *Adv. Opt. Mater.* **2021**, *9*, 2001745.
[19] H. Kim, W. J. Lee, A. C. Farrell, A. Balgarkashi, D. L. Huffaker, *Nano Lett.* **2017**, *17*, 5244.
[20] H. Kim, W. J. Lee, A. C. Farrell, J. S. D. Morales, P. Senanayake, S. V. Prikhodko, T. J. Ochalski, D. L. Huffaker, *Nano Lett.* **2017**, *17*, 3465.
[21] T. Chang, H. Kim, B. T. Zutter, W. Lee, B. C. Regan, D. L. Huffaker, *Adv. Funct. Mater.* **2020**, *30*, 2002220.
[22] P. Schmiedeke, A. Thurn, S. Matich, M. Döblinger, J. J. Finley, G. Koblmüller, *Appl. Phys. Lett.* **2021**, *118*, 221103.
[23] W. J. Lee, H. Kim, A. C. Farrell, P. Senanayake, D. L. Huffaker, *Appl. Phys. Lett.* **2016**, *108*, 081108.
[24] L. H. Wu, X. Hu, *Phys. Rev. Lett.* **2015**, *114*, 223901.
[25] M. Minkov, I. A. D. Williamson, L. C. Andreani, D. Gerace, B. Lou, A. Y. Song, T. W. Hughes, S. Fan, *ACS Photonics* **2020**, *7*, 1729.
[26] N. Susa, *J. Appl. Phys.* **2000**, *89*, 815.
[27] P. Staudinger, K. E. Moselund, H. Schmid, *Nano Lett.* **2020**, *20*, 686.
[28] N. Goktas, V. Dubrovskii, R. LaPierre, *J. Phys. Chem. Lett.* **2021**, *12*, 1275.
[29] O. Arif, V. Zannier, A. Li, F. Rossi, D. Ercolani, F. Beltramand, L. Sorba, *Cryst. Growth Des.* **2020**, *20*, 1088.
[30] F. Ishizaka, Y. Hiraya, K. Tomioka, J. Motohisa, T. Fukui, *Nano Lett.* **2017**, *17*, 1350.
[31] J. Treu, M. Bormann, H. Schmeiduch, M. Döblinger, S. Morkötter, S. Matich, P. Wiecha, K. Saller, B. Mayer, M. Bichler, M. C. Amann, J. J. Finley, G. Abstreiter, G. Koblmülle, *Nano Lett.* **2013**, *13*, 6070.
[32] L. Balaghi, G. Bussone, R. Grifone, R. Hübner, J. Grenzer, M. Ghorbani-Asl, A. V. Krasheninnikov, H. Schneider, M. Helm, E. Dimakis, *Nat. Commun.* **2019**, *10*, 2793.
[33] M. Zamani, G. Tütüncüoglu, S. Sánchez, L. Francaviglia, L. Güniat, L. Ghisalberti, H. Potts, M. Friedl, E. Markov, W. Kim, J. B. Leran, V. G. Dubrovskii, J. Arbiol, A. F. i Morral, *Nanoscale* **2018**, *10*, 17080.
[34] P. Staudinger, S. Mauthe, K. E. Moselund, H. Schmid, *Nano Lett.* **2018**, *18*, 7856.
[35] J. Johansson, L. Karlsson, C. Svensson, T. Martensson, B. Wacaser, K. Deppert, L. Samuelson, W. Seifert, *Nat. Mater.* **2006**, *5*, 574.
[36] R. E. Nahory, M. A. Pollack, W. D. Johnston, R. L. Barns, *Appl. Phys. Lett.* **1978**, *33*, 659.
[37] M. Imada, A. Chutinan, S. Noda, M. Mochizuki, *Phys. Rev. B* **2002**, *65*, 195306.
[38] C. Degen, I. Fischer, W. Elsäßer, J. Vey, P. Schnitzer, *Opt. Express* **1999**, *5*, 38.